



Article

A Low-Complexity Model-Free Approach for Real-Time Cardiac Anomaly Detection Based on Singular Spectrum Analysis and Nonparametric Control Charts

Michael Lang 

Graduate School of Excellence Computational Engineering, Technische Universität Darmstadt, Dolivostraße 15, 64293 Darmstadt, Germany; michael.lang@ieee.org; Tel.: +49-6151-1624401; Fax: 49-6151-1624404

Received: 11 December 2017; Accepted: 13 February 2018; Published: 15 February 2018

Abstract: While the importance of continuous monitoring of electrocardiographic (ECG) or photoplethysmographic (PPG) signals to detect cardiac anomalies is generally accepted in preventative medicine, there remain numerous challenges to its widespread adoption. Most notably, difficulties arise regarding crucial characteristics such as real-time capability, computational complexity, the amount of required training data, and the avoidance of too-restrictive modeling assumptions. We propose a lightweight and model-free approach for the online detection of cardiac anomalies such as ectopic beats in ECG or PPG signals on the basis of the change detection capabilities of singular spectrum analysis (SSA) and nonparametric rank-based cumulative sum (CUSUM) control charts. The procedure is able to quickly detect anomalies without requiring the identification of fiducial points such as R-peaks, and it is computationally significantly less demanding than previously proposed SSA-based approaches. Therefore, the proposed procedure is equally well suited for standalone use and as an add-on to complement existing (e.g., heart rate (HR) estimation) procedures.

Keywords: nonparametric change point detection; singular spectrum analysis; cumulative sums; ECG; PPG; arrhythmias; cardiac monitoring

1. Introduction

The ubiquity of powerful smartphones and other smart devices, which nowadays incorporate a plethora of advanced sensing capabilities, has led to an increasing trend in the consumer sphere to continuously gather and evaluate physiological signals [1,2]. In particular, cardiovascular parameters such as heart rate (HR) and pulse rate (PR), extracted respectively from measurements of myocardial electrical potentials through electrocardiographic (ECG) observations [3–6] and from measurements of volumetric changes in blood perfusion during cardiac cycles by optical means through photoplethysmographic (PPG) observations [7–9], are being recorded and analyzed in apps, fitness trackers and so forth, with great potential benefits for public health [1,10–12].

Virtually all of such consumer-oriented apps and devices fall into the category of fitness and well-being products, thereby avoiding the substantial burden of having to comply with requirements imposed by medical device regulatory frameworks [13,14], which is reflected by often notoriously inaccurate and unreliable results [15,16]. Moreover, functionality is usually limited to providing estimates of the average HR.

While low-resolution averaged HR estimates may be of some use in fitness and well-being scenarios, from a clinical perspective, the detection of sudden changes in the signal structure is of the utmost importance. ECG recordings from a healthy heart are characterized by a sinus rhythm,

wherein the normal cardiac cycle begins with an action potential in the sinoatrial (SA) node, located in the right atrium, which propagates and depolarizes neighboring cells. The depolarization of the SA node spreads rapidly throughout both atria, specifically to the left atrium through Bachmann's bundle and through internodal pathways in the right atrium to the atrioventricular (AV) node. Full depolarization gives rise to the P-wave, which initiates atrial contraction. From the AV node, excitation is further propagated after an initial delay of about 100 ms through the bundle of His, which splits up into the right bundle branch and the left bundle branch, initiating respectively the depolarization of the right and left ventricle, yielding to the conspicuous QRS-complex, which ends with completely depolarized and contracting ventricles. Ventricular repolarization following the contraction eventually results in the T-wave and concludes the normal cardiac cycle. We note that both left and right bundle branches eventually differentiate into a large number of Purkinje fibers, the repolarization of which is thought to occasionally result in an additional U-wave [3].

Deviations from the normal sinus rhythm are referred to as arrhythmias and comprise a large number of specific arrhythmias (see, e.g., [17]). Heart rhythms exhibiting variations in timing, such as those that are either below 60 beats per minute (bpm) or above 100 bpm, as well as rhythms disrupted by changes in the morphology, for example, as a result of ectopic beats (i.e., heart beats whose origin is different from and outside of the region typically responsible for impulse generation, namely, the SA node) such as premature ventricular contractions (PVCs) or premature atrial contractions (PACs), all qualify as arrhythmias. Furthermore, they all tend to induce distinctive changes in the ECG signal, thereby allowing for a change detection approach, which must not necessarily be based on templates corresponding to the various arrhythmia-induced changes [18]. Additionally, many arrhythmias, although usually not acutely life-threatening, are paroxysmal and asymptomatic and therefore likely to go unnoticed for long periods of time, which carries the risk of exacerbation and possibly the development of more serious types of arrhythmias [3,17,18]. Outpatient cardiac monitoring through wearable devices and apps is commonly accepted as a promising approach to tackle this issue and improve treatment outcome while at the same time lowering overall healthcare costs [1,10–12,18,19].

The automatic monitoring of ECG signals has been researched for decades, and various algorithms have been proposed and implemented. However, the shift towards outpatient monitoring through low-power wearable devices and apps introduces additional challenging requirements such as real-time capability, the ability to cope with rather noisy and low-quality signals with various artifacts, and harsh constraints on computational complexity and power consumption [18–20]. Various approaches for the automatic online detection of cardiac arrhythmias have been proposed in the literature. Machine learning approaches have been adopted by numerous authors [21,22], and as have wavelet- [22,23], artificial neural network (ANN)- [24–26], and decision tree-based [27] approaches. For a more detailed review, the reader is referred to recent review papers [18,28]. Most approaches require the extraction of certain features from the signal, such as the location of QRS complexes [20,27,29,30] or R-peaks [22,23,31–33]. This is commonly performed using the algorithm proposed by Pan and Tompkins [34] or variations thereof [18,28], resulting in an inherent vulnerability to inaccuracies in the initial estimation of these fiducial points. The reliance upon rather restrictive modeling assumptions and the requirement of large amounts of training data is not uncommon. On the other hand, recent research has resulted in improved and numerically efficient QRS detectors that are particularly suited for mobile battery-powered applications. Among the latter, we point out the fast QRS detection algorithm proposed by Elgendi [35], as well as the general two event-related moving averages (TERMA) framework [36] by the same author, for being highly efficient, yet much simpler and faster than conventional QRS detectors. It is furthermore worth noting that Elgendi and colleagues in [37] and more recently in [38] were able to show the good performance characteristics of TERMA-based QRS detectors to also hold for compressed ECG signals. In particular, in [38], they were able to corroborate this for ECG records decimated by a factor of up to 8, making TERMA-based QRS detectors particularly well suited for mobile health applications in low- and middle-income countries (see also [39]).

We propose a lightweight and model-free approach for the online detection of cardiac anomalies such as ectopic beats in ECG or PPG signals on the basis of the change detection capabilities of singular spectrum analysis (SSA) and nonparametric rank-based cumulative sum (CUSUM) control charts. The procedure is able to quickly detect anomalies without requiring templates, extensive training data sets or the identification of fiducial points such as R-peaks. This is accomplished by leveraging the power and versatility of SSA to capture the essential signal structure as well as potential changes therefrom. We note that, crucially and contrary to the aforementioned QRS detectors, this is achieved without requiring a morphological dissection of the signal. From a computational complexity perspective, while our proposed method is certainly more involved than a QRS detector, it is significantly less demanding than previously proposed SSA approaches.

The proposed method is essentially composed of two consecutive steps: a SSA-based algorithm is sequentially applied to the observed data to construct viable test statistics that reflect potential changes in the cardiac signal, and these statistics are then monitored using distribution-free CUSUM-type control charts.

The use of SSA in a sequential framework as a means for change detection as introduced in Section 2 is based on works by Moskvina and Zhigljavsky, discussed in detail in [40] and in a more condensed fashion in [41], although it should be noted that the concept was already described earlier in [42]. This algorithm has successfully been applied to various real-world detection problems, for example, anomaly detection in cognitive radio networks [43], smart power grids [44], software engineering [45] and change point detection for complex-valued time series [46]. In the biomedical context, it has shown to be useful for the identification of freezing of gait in patients with Parkinson's disease [47], and the detection of anomalies in periodic biosignals such as ECGs [48], as well as in other biomedical applications [49].

Building on the prior technique outlined in Section 2, we introduce a novel SSA-based change detection procedure (lightweight singular spectrum analysis change point detection: l-SSA-CPD) that exhibits good performance characteristics while at the same time drastically reduces the computational burden. As is shown in Section 3, this is accomplished by modifying the conventional SSA-based change detection algorithm such that the computationally expensive task of computing the singular value decomposition (SVD) is only performed at the very beginning instead of each time a new data point becomes available. Furthermore, the proposed procedure uses more elaborate test statistics that take into account the information derived from the angle between data vectors representing new observations and the subspace representing the signal characteristics as well as the Euclidean distances. Lastly, our procedure differs from previous approaches also in that rank-based control limits and the reinitialization of control charts after an anomaly has been detected are used.

A performance evaluation of l-SSA-CPD using ECG and PPG records from the publicly available Physionet Challenge 2015 training database (PC15) [50,51] are presented in Section 4.3 and compared to a recently proposed competing algorithm by Pflugradt et al. [52].

Furthermore, we evaluate the performance of our simpler method against that of a previously published work by Uus and Liatsis [48], which is related to our work in that it, too, is based on leveraging the change detection capabilities of SSA. For the latter assessment, we used 10 cardiologist-annotated ECG records from the St. Petersburg Institute of Cardiological Technics 12-Lead Arrhythmia (INCART) database, which is also publicly available through Physiobank [51]. These results are presented and elaborated on in Section 4.4 and are eventually followed by a short discussion in Section 5, which concludes this paper.

2. Singular Spectrum Analysis

2.1. Fundamentals of Singular Spectrum Analysis

SSA is a technique of time series analysis and can be interpreted as belonging to the general class of principal component analysis (PCA) methods. SSA has become a standard tool in meteorology and

climatology but is mostly unknown outside of those disciplines. Golyandina et al. [42] attribute this to the nature of SSA being more a technique of multivariate geometry than of statistics. According to their representation, SSA should rather be seen as an exploratory, model-building tool than a confirmatory procedure. In essence, SSA can be seen as the application of PCA to the “trajectory matrix” (obtained directly from the original time series) with the subsequent attempt to reconstruct the original series. Prior to proceeding to SSA for change detection, a short introduction to the basic SSA algorithm appears in order.

2.1.1. Basic SSA Algorithm

Consider N observations $\mathbb{X}_N = (x_1, \dots, x_N)$ of a univariate time series and an integer M ($1 < M \ll N$) commonly referred to as the *window length*, *lag-integer* or *embedding dimension*. The basic SSA algorithm is commonly described as being composed of the following four stages (see, e.g., [42,49,53]):

1. Embedding: $\mathbb{X}_N = (x_1, \dots, x_N) \rightarrow \mathbf{X} \in \mathbb{R}^{M \times K}$

A trajectory matrix \mathbf{X} is constructed by mapping \mathbb{X}_N into a sequence of $K = N - M + 1$ lagged column vectors $X_j = (x_j, \dots, x_{j+M-1})^T, j = 1, \dots, K$ of size M , yielding

$$\mathbb{X}_N = (x_1, x_2, \dots, x_N) \rightarrow \mathbf{X} = \begin{bmatrix} x_{n+1} & x_{n+2} & \dots & x_{n+K} \\ x_{n+2} & x_{n+3} & \dots & x_{n+K+1} \\ \vdots & \vdots & \ddots & \vdots \\ x_{n+M} & x_{n+M+1} & \dots & x_{n+N} \end{bmatrix}. \quad (1)$$

Notice the *Hankel-structure* of $\mathbf{X} = (x_{ij})_{i,j=1}^{M,K}$, i.e., \mathbf{X} has equal elements on the anti-diagonals $i + j = \text{const}$.

One can think of \mathbf{X} as multivariate data with M characteristics and K observations and accordingly X_j of \mathbf{X} as vectors in the M -dimensional space \mathbb{R}^M .

2. Singular Value Decomposition of \mathbf{X}

Taking the SVD of \mathbf{X} decomposes the trajectory matrix into its orthogonal bases and yields a collection of M eigenvalues and eigenvectors. Let $\lambda_1 \geq \dots \geq \lambda_M \geq 0$ and U_1, \dots, U_M denote, respectively, the eigenvalues and eigenvectors of $\mathbf{X}\mathbf{X}^T$ and the *rank* of \mathbf{X} be denoted as $d = \max(i, \text{such that } \lambda_i > 0)$. The SVD of \mathbf{X} can then be rewritten as the sum of d elementary matrices

$$\mathbf{X} = \mathbf{X}_1 + \dots + \mathbf{X}_d, \quad (2)$$

with matrices $\mathbf{X}_i = \sqrt{\lambda_i} U_i V_i^T$ being of rank 1 and $V_i = \mathbf{X}^T U_i / \sqrt{\lambda_i}$.

Note that V_i are the eigenvectors of $\mathbf{X}^T \mathbf{X}$ and $(\sqrt{\lambda_i}, U_i, V_i)$ the *eigen triples* of the SVD in Equation (2).

Also note that due to the symmetry of left and right singular vectors, the SVD of trajectory matrices obtained with window length M and $K = N - M + 1$ are equivalent. Accordingly, one can impose the limitation $M \leq N/2$ on the window length since there is no additional benefit in using a larger window (see, e.g., [53] at 47, [42] at 69).

3. Eigen triple Grouping

In order to separate the signals of interest from noise and artifacts, the third stage of basic SSA aims to find particular disjoint subsets of the set of indices $\{1, \dots, d\}$ such that the respective systems of eigenvectors span the subspaces associated with the different signal components.

Consider the task of separating a signal of interest from unwanted noise. One then looks for a certain subset of indices $I = \{i_1, \dots, i_l\}, l < d \leq M$ that span an l -dimensional subspace in \mathbb{R}^M ,

denoted as $\mathcal{L}_I \subset \mathbb{R}^M = \text{span}\{U_I\} = \text{span}\{U_{i_1}, \dots, U_{i_l}\}$. Analogously, the remaining eigentriples with $\bar{I} = \{i_1, \dots, i_d\} \setminus I$ span the noise subspace $\mathcal{L}_{\bar{I}} \subset \mathbb{R}^M = \text{span}\{U_{\bar{I}}\}$.

The trajectory matrix component \mathbf{X}_I corresponding to the subset I of eigentriples associated with the signal of interest is then

$$\mathbf{X}_I = \mathbf{X}_{i_1} + \dots + \mathbf{X}_{i_l} \quad (3)$$

and the component $\mathbf{X}_{\bar{I}}$ corresponding to the subset $\bar{I} = \{i_1, \dots, i_d\} \setminus I$ associated with the remainder of the observed signal is

$$\mathbf{X}_{\bar{I}} = \sum_{i \in \bar{I}} \mathbf{X}_i, \quad (4)$$

such that

$$\mathbf{X} = \mathbf{X}_I + \mathbf{X}_{\bar{I}} = \sum_{i \in I} \mathbf{X}_i + \sum_{i \in \bar{I}} \mathbf{X}_i. \quad (5)$$

In the case of separability (see, e.g., [53] at 17), the contribution of \mathbf{X}_I to the entire observed signal \mathbf{X} is represented by the respective share of eigenvalues $\sum_{i \in I} \lambda_i / \sum_{i=1}^d \lambda_i$.

4. Diagonal Averaging

For perfectly separable components, all matrices in the expansion of Equation (5) are Hankel matrices. For real world problems, however, such perfect separability is rarely achievable and results in matrices with unequal entries on the antidiagonals. The last step of the basic SSA algorithm therefore performs a Hankelization of said matrices, i.e., a diagonal averaging is performed on all the \mathbf{X}_i of Equation (5) yielding matrices $\tilde{\mathbf{X}}_i$ that have equal elements on the antidiagonals

$$\tilde{\mathbf{X}} = \tilde{\mathbf{X}}_I + \tilde{\mathbf{X}}_{\bar{I}} = \sum_{i \in I} \tilde{\mathbf{X}}_i + \sum_{i \in \bar{I}} \tilde{\mathbf{X}}_i. \quad (6)$$

One can then e.g., easily reconstruct the approximation of the signal of interest through the eigentriples with indices I through the one-to-one correspondence between $\tilde{\mathbf{X}}_I$ and the respective time series $\tilde{\mathbb{X}}_N = (\tilde{x}_1, \dots, \tilde{x}_N)$ which provides an approximation of the entire time series \mathbb{X}_N or some components of it, depending on the particular choice of indices I .

The usefulness of basic SSA is illustrated in the example depicted in Figure 1 where the wandering baseline of an ECG signal (blue solid line) is removed by subtracting the trend reconstructed through SSA (with a window length of $M = 100$ and using the first two eigentriples $\tilde{\mathbf{X}}_I = \tilde{\mathbf{X}}_{i_1} + \tilde{\mathbf{X}}_{i_2} \rightarrow \tilde{\mathbb{X}}_N = (\tilde{x}_1, \dots, \tilde{x}_N)$ (red solid line)) from the original signal, i.e.,

$$\mathbb{X}_{N_{\text{cleaned}}} = \mathbb{X}_N - \tilde{\mathbb{X}}_N = (x_1, \dots, x_N) - (\tilde{x}_{i_{11}}, \dots, \tilde{x}_{i_{1N}}) - (\tilde{x}_{i_{21}}, \dots, \tilde{x}_{i_{2N}}), \quad (7)$$

yielding the cleaned ECG signal (green solid line).

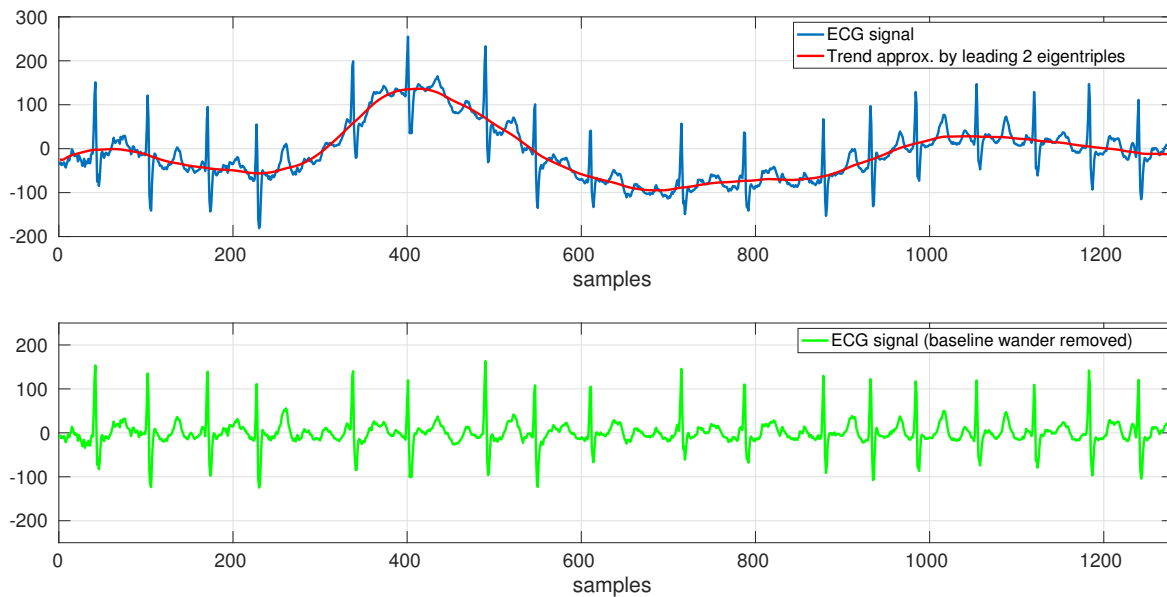


Figure 1. Application example of basic SSA: baseline wander removal. Showing excerpt 02:20–02:30 from record 14,149 m MIT-BIH ltdb [51].

For a more detailed discussion of SSA, we refer to two well-known monographs [42,54] in the field as well as [49,53] and references therein.

2.2. SSA Based Change Detection: Prior Art

The sequential application of SSA described in the following is based on work by Moskvina and Zhigljavsky and will be referred to as MZ in the remainder of this paper (see [40–42]). The need for an adaptation of basic SSA is due to the circumstance that it operates in batch mode and is therefore not suited for online change-point detection.

Assume a truly sequential problem in which observations x_1, x_2, \dots arrive one at a time. Having collected a sufficiently large number N of observations, MZ constructs the trajectory matrix $\mathbf{X}_B^{(n)}$ (the subindex B refers to ‘base’ for reasons that will become obvious in a moment) for time index n with $M \leq N/2, K = N - M + 1$ and performs the SVD and grouping steps as in basic SSA yielding an l -dimensional subspace $\mathcal{L}_I^{(n)} \subset \mathbb{R}^M$ spanned by the respective eigenvectors which captures the main structure of the signal.

The basic idea of MZ relies on the fact that the distance between the vectors $X_j^{(n)}, j = 1, \dots, K$ and $\mathcal{L}_I^{(n)}$, controlled by the specific choice of I , can be reduced to rather small values. If monitoring of the series $\{x_t\}_{t=1}^N$ continues for $t > N$ without a change in the underlying data generating mechanism, the vectors $X_j, j > K$ are expected to remain relatively close to $\mathcal{L}_I^{(n)}$ while, on the other hand, if such a change were to occur at time $N + \tau$, the distance between $X_j, j \geq K + \tau$ and \mathcal{L}_I would increase as it would move such vectors X_j out of the subspace $\mathcal{L}_I^{(n)}$ (see [41] at 2). Therefore, said distance can be used as a test statistic for change-point detection. Note that only the first three steps of basic SSA need to be performed since reconstruction of the original series is not required.

MZ constructs two matrices, the above mentioned *base matrix* $\mathbf{X}_B^{(n)}$, i.e., the trajectory matrix using data samples x_{n+1}, \dots, x_{n+N} , and a *test matrix* $\mathbf{X}_T^{(n)}$ using observations $x_{n+p+1}, \dots, x_{n+q+M-1}$. The former is subjected to SVD and used to obtain the subspace $\mathcal{L}_I^{(n)}$ while the latter serves to calculate the sum of squared Euclidean distances between its column vectors and $\mathcal{L}_I^{(n)}$. This process can be thought of as having two (possibly intersecting) windows (of M -dimensional data), of length K and $Q = q - p$ respectively, slide over the data.

Let N, M, l, p, q be fixed integers s.t. $l < M < N/2$ and $0 \leq p < q$. Then, for each $n = 0, 1, \dots$ MZ proceeds as follows:

1. Apply SSA on the interval $[n + 1, n + N]$ (after centering x_{n+1}, \dots, x_{n+N}) to get $\mathcal{L}_I^{(n)}$

- (a) Construct the trajectory/base matrix $\mathbf{X}_B^{(n)}$

$$\mathbf{X}_B^{(n)} = \begin{bmatrix} x_{n+1} & x_{n+2} & \dots & x_{n+K} \\ x_{n+2} & x_{n+3} & \dots & x_{n+K+1} \\ \vdots & \vdots & \ddots & \vdots \\ x_{n+M} & x_{n+M+1} & \dots & x_{n+N} \end{bmatrix}, \quad (8)$$

where $K = N - M + 1$.

- (b) Singular Value Decomposition of $\mathbf{X}_B^{(n)}$.

- (c) Selection of $l = \{i_1, \dots, i_l\}, l < d \leq M$ with $d = \max(i, \text{such that } \lambda_i > 0)$.

2. Construct test matrix $\mathbf{X}_T^{(n)}$ on the interval $[n + p + 1, n + q + M - 1]$ (after centering $x_{n+p+1}, \dots, x_{n+q+M-1}$)

$$\mathbf{X}_T^{(n)} = \begin{bmatrix} x_{n+p+1} & x_{n+p+2} & \dots & x_{n+q} \\ x_{n+p+2} & x_{n+p+3} & \dots & x_{n+q+1} \\ \vdots & \vdots & \ddots & \vdots \\ x_{n+p+M} & x_{n+p+M+1} & \dots & x_{n+q+M-1} \end{bmatrix}. \quad (9)$$

3. Compute the detection statistic $D_{n,l,p,q}$

$$D_{n,l,p,q} = \sum_{j=p+1}^q \left[\left(X_j^{(n)} \right)^T X_j^{(n)} - \left(X_j^{(n)} \right)^T \mathbf{U}_I^{(n)} \left(\mathbf{U}_I^{(n)} \right)^T X_j^{(n)} \right], \quad (10)$$

where $X_j^{(n)} = [x_{n+j}, \dots, x_{n+j+M-1}]^T$ and $\mathbf{U}_I^{(n)} = [U_{i_1}^{(n)}, \dots, U_{i_l}^{(n)}]$ is the $M \times l$ matrix of eigenvectors spanning $\mathcal{L}_I^{(n)}$, i.e., $D_{n,l,p,q}$ is the sum of squared Euclidean distances between the columns of $\mathbf{X}_T^{(n)}$ and $\mathcal{L}_I^{(n)}$. MZ normalizes the sum of distances $D_{n,l,p,q}$ to the number of elements in $\mathbf{X}_T^{(n)}$, i.e.,

$$\tilde{D}_{n,l,p,q} = \frac{D_{n,l,p,q}}{MQ}, \quad (11)$$

and further normalizes the test statistic as

$$S_{n,l,p,q} = \frac{\tilde{D}_{n,l,p,q}}{v_n} \quad (12)$$

such that it does not depend on the unknown variance of the noise (see [40] at 28) with v_n being an estimator of $\tilde{D}_{n,l,p,q}$, e.g., $v_n = \tilde{D}_{m,l,0,K}$ with $m \leq n$ such that the hypothesis of no change can be accepted.

4. Monitoring of $S_{n,l,p,q}$ using CUSUM-type Control Charts

MZ then constructs the following CUSUM-type control chart:

$$W_1 = S_{1,l,p,q}, \quad W_{n+1} = \max(0, W_n + S_{n+1,l,p,q} - S_{n,l,p,q} - \kappa), \quad n \geq 1, \quad (13)$$

with κ suggested as $\kappa = 1 / (3\sqrt{MQ})$ (see [40] at 29) and threshold $h_{MZ} = 1 + 1.9\sqrt{M}$ (see [40] at 35). A change-point at n is then declared if

$$W_n \geq h_{MV} \quad (14)$$

holds.

3. The Proposed Method (l-SSA-CPD)

While MZ provides a powerful methodology that could be applied directly to raw ECG (or PPG) data, it exhibits some drawbacks (for the particular application at hand) that motivated the development of the novel approach to be presented below which we shall refer to as *lightweight-SSA-ChangePointDetection* (l-SSA-CPD).

3.1. Motivation and Informal Description of the Improvements

As discussed in the preceding Section, MZ makes use of two (possibly intersecting) windows that are slid over the observed time series, one comprising the data that is embedded to form the trajectory matrix, which is then decomposed by means of SVD to identify an appropriate low(er)-dimensional subspace, and another one containing new (or, in case of overlap, a combination of old and new) observations whose distance to said low-dimensional subspace is then used as a test statistic. This entails the quite burdensome step of performing a SVD every time a new data sample becomes available.

We shall first highlight the main improvements of our method prior to its formal description.

- Low Computational Complexity

Small variations over time are intrinsic to cardiac signals and may, besides noise and motion artifacts, e.g., be due to *Heart Rate Variability*. Contrary to anomalies caused by abnormal cardiac excitation phenomena, these changes in the time between consecutive R-peaks are subtle and often not readily discernible. Most importantly, they do not induce changes as severe as to change the signal's main characteristics which are captured through the decomposition and grouping stages of SSA. This is illustrated in Figure 2 which shows a raw (unfiltered) ECG signal with two distinctly shaped PVCs (highlighted in purple) in the third quarter of the excerpt.

For the task at hand, performing the SVD of a newly generated trajectory matrix each time a new data point becomes available is not strictly necessary. We are able to drastically reduce the computational burden by generating only one initial trajectory matrix $\mathbf{X}_B^{(0)}$ and relying on the obtained reference subspace $\mathcal{L}_I^{(0)}$ throughout the monitoring. This is shown in Figure 2 with the section of the signal highlighted through gray and blue backgrounds representing the intervals used to generate $\mathbf{X}_B^{(n)}$ and $\mathbf{X}_T^{(n)}$, respectively. Note how in MZ (left part of Figure 2) both $\mathbf{X}_B^{(n)}$ and $\mathbf{X}_T^{(n)}$ are being slid over the observations while in our algorithm (right part of Figure 2) only $\mathbf{X}_T^{(n)}$ is a sliding window since $\mathbf{X}_B^{(n)}|_{\forall n} = \mathbf{X}_B^{(0)}$.

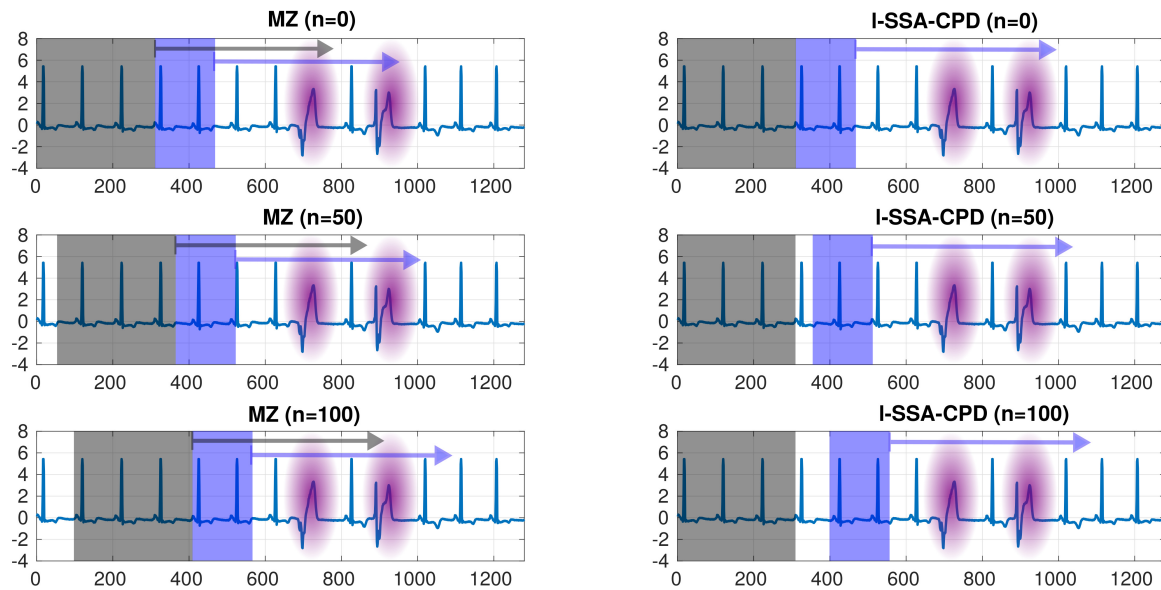


Figure 2. Comparison of MZ (left) and I-SSA-CPD (right). The computational burden of I-SSA-CPD is greatly reduced compared to MZ by relying on the reference subspace obtained from an initial, non-sliding trajectory matrix (illustrated by the gray background area). Furthermore, note that I-SSA-CPD's reference subspace remains locked on the main signal's characteristics while in MZ, since the reference subspace is updated at each observation (illustrated by the gray area sliding as well), it will lock on the two anomalies (highlighted in pink) for some time as the two moving windows are pass over them.

Clearly, relying on a fixed reference subspace $\mathcal{L}_I^{(0)}$ throughout the entire monitoring process goes along with an inherent limitation of the potential application scenarios I-SSA-CPD would be suited for as it implies the fixed nominal subspace to be a valid representation of the anomaly free signal over long periods of time. While such an assumption may at first appear extreme and untenable, this is not the case when monitoring subjects at rest over relatively short periods of time (e.g., in the order of 2–10 min) as would be the case in a typical prescreening scenario for ambulatory care settings. Said implied assumption however becomes untenable in other relevant scenarios such as continuous long-term monitoring as well as the monitoring of patients not at rest; for in those cases the general cardiovascular responses to homeostatic disturbances triggered by various physical and mental stressors would suffice to move new observations out of the designated nominal subspace.

There exist, however, various rather straightforward mitigation strategies to this problem. For instance, we may view the method presented here as a special case of a more general I-SSA-CPD that allows for the regular recalculation of the reference subspace according to an update frequency which depends on the particular scenario. Possibilities to lower the computational burden on the mobile device are equally manifold and include, among others, establishing a wireless data connection to a server or PC and outsourcing demanding tasks such as SVD or substituting SVD with a computationally less expensive alternative such as SVD updating algorithms. Eventually, such considerations inevitably boil down to a scenario specific trade-off between required performance and available resources.

- **Simplicity**

By sliding only a single instead of two windows over the time series the entire procedure is simplified and benefits from a reduction in tuning parameters.

In fact, while the total number Q of columns in \mathbf{X}_T is of course relevant, p and q are not since, due to $\mathbf{X}_B^{(n)}|_{\forall n} = \mathbf{X}_B^{(0)}$ an overlap of \mathbf{X}_B and \mathbf{X}_T can only occur in the first $N - p$ samples for $p < N$.

While our algorithm allows for such an initial overlap of \mathbf{X}_B and \mathbf{X}_T , the following discussion is purposely limited to $p = N < q$, which is in line with recommendations by Moskvina and Zhigljavsky who point out that $p = N, q = N + 1$ and accordingly $Q = 1$ is a very reasonable choice if minimizing the detection delay is of importance, since $Q > 1$ entails a smoother behavior of the test statistic and thus a loss of agility (see, e.g., [40] at 30).

The question as to whether or not \mathbf{X}_B and \mathbf{X}_T should overlap and if so by how much is therefore removed. Furthermore, since $p = N, q = N + 1$ can generally be recommended (see Section 4), we can omit both tuning parameters p and q .

- Augmentation of Test Statistic by considering the angle between $\mathcal{L}_I^{(0)}$ and $X_j^{(n)}$

Some authors [55–57] successfully proposed a modified version of MZ, wherein the test statistic is based on angles rather than on Euclidean distances. While both approaches are viable on their own merits, we chose to merge them as they augment each other yielding a test statistic that, according to our results on raw ECG and PPG records, performs favorably compared to the test statistic constructed using either one on its own.

In other words, we augment and improve upon the test statistic of MZ by making use of the information from the angles between $\mathcal{L}_I^{(0)}$ and $X_j^{(n)}$ as well.

- Improved thresholding through Sequential Ranks CUSUM

MZ provides further potential for improvement by employing a CUSUM-type control chart (see Equations (13) and (14)) whose control limit (or threshold) h is obtained through suitable normal approximation and asymptotic considerations (see [40] at 31; see also [41] at 8). The nuisance of having to properly normalize the test statistic (see Equation (12)) is a direct consequence of this design choice.

We instead propose the use of McDonald's Sequential Ranks CUSUM (SRC) [58] which we deem to be more appropriate and in line with the model-free nature of SSA.

- Restarting of SRC control chart after it signaled

Lastly, to allow for the detection of multiple and potentially nearby change-points we restart the SRC every time after it signaled an anomaly by exceeding the preset threshold h_{SRC} .

This is indicated since otherwise, depending on the extent of the anomaly (in terms of number of samples) and how it relates to the embedding dimension M as well as the number Q of columns in the Hankel matrix \mathbf{X}_T , it may take some time before the anomaly propagates through and clears \mathbf{X}_T (i.e., our sliding window) thereby resulting in a return of the test statistic to its 'baseline level'. This is illustrated in Figure 3 where, as depicted in (a), three windows (differing in size) with $Q = \{1, 20, 40\}$ are slid over an ECG containing a single PVC (highlighted in purple and marked with an arrow). As can be seen in (b), while $Q = 1$ is a feasible choice even without restarting the control chart after exceeding the threshold h_{SRC} , since the respective SRC returns to values below h_{SRC} after a relatively long but perhaps still acceptable amount of time, the same cannot be said for $Q = \{20, 40\}$. Part (c) of Figure 3 illustrates the clear benefits of restarting the control charts, in that regardless of the choice of Q the PVC is detected and monitoring for further changes can swiftly resume. As was to be expected, $Q = 1$ is favorable in terms of detection delay.

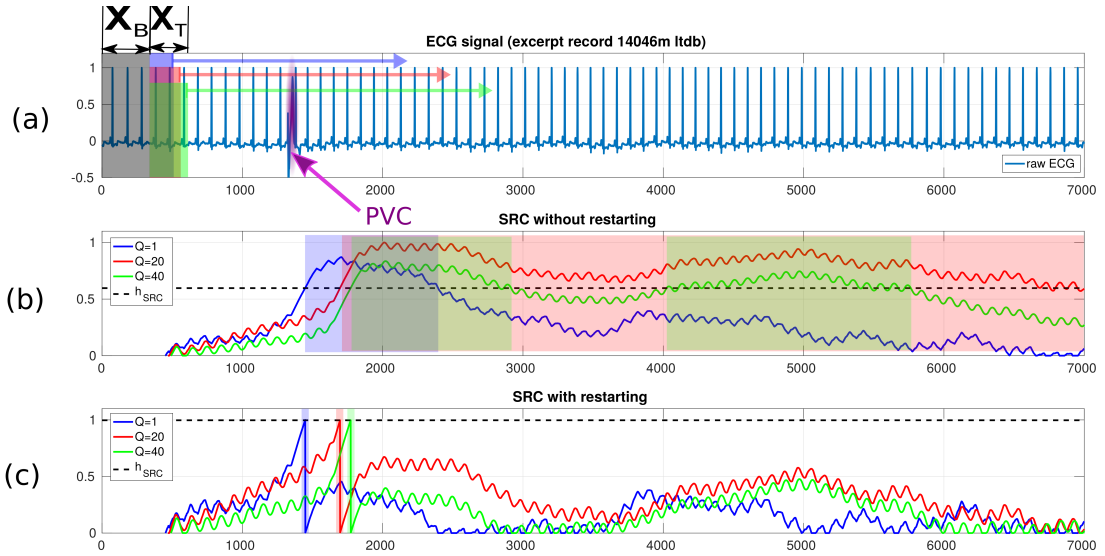


Figure 3. Whilst monitoring the ECG signal (a), restarting the SRC each time the threshold was hit (c) is indicated to avoid potentially lengthy delays before the anomaly propagates through and clears X_T (b).

3.2. Formal Description of l-SSA-CPD

To allow for better comparison, we use the notation introduced in Section 2.2 as far as possible.

Let N, M, l, p, q be fixed integers s.t. $l < M < N/2$ and $0 \leq p < q$. Then our method proceeds as follows:

1. Initialization at $n = 0$

SSA is applied on the interval $[n + 1, n + N]$ to get $\mathcal{L}_I = \mathcal{L}_I^{(n=0)}$, which akin to MZ involves:

- (a) Construction of the trajectory/base matrix $\mathbf{X}_B = \mathbf{X}_B^{(0)} = \mathbf{X}_B^{(n=0)}$, see Equation (8).
- (b) Singular Value Decomposition of \mathbf{X}_B .
- (c) Selection of $I = \{i_1, \dots, i_l\}, l < d \leq M$ with $d = \max(i, \text{such that } \lambda_i > 0)$.

Then, for each $n = 0, 1, \dots$ we proceed as follows:

2. Construct test matrix $\mathbf{X}_T^{(n)} = \left[X_{j|j=p+1, \dots, q}^{(n)} \right]$ on the interval $[n + p + 1, n + q + M - 1]$, see Equation (9).
3. Compute the detection statistics $D_{n,l,p,q}^{\dagger_{1, \dots, 3}}$

$$D_{n,l,p,q}^{\dagger_1} = \frac{1}{Q} \sum_{j=p+1}^q \left[\left(X_j^{(n)} \right)^T X_j^{(n)} - \left(X_j^{(n)} \right)^T \mathbf{U}_I \left(\mathbf{U}_I \right)^T X_j^{(n)} \right], \quad (15)$$

$$D_{n,l,p,q}^{\dagger_2} = 1 - \cos \left[\angle \left(\mathbf{X}_T^{(n)}, \mathcal{L}_I \right) \right], \quad (16)$$

$$D_{n,l,p,q}^{\dagger_3} = D_{n,l,p,q}^{\dagger_1} \circ D_{n,l,p,q}^{\dagger_2}, \quad (17)$$

with

$$\angle(\mathbf{X}_T^{(n)}, \mathcal{L}_I) = \angle(\mathbf{X}_T^{(n)}, \mathbf{U}_I) = \frac{1}{Q} \sum_{j=p+1}^q \frac{1}{l} \left[\sum_{k=i_1}^{i_l} \arccos \left(\frac{\langle \mathbf{X}_j^{(n)}, \mathbf{U}_k \rangle}{\|\mathbf{X}_j^{(n)}\| \|\mathbf{U}_k\|} \right) \right] \quad (18)$$

taking values in $[0, \frac{\pi}{2}]$, accordingly $D_{n,l,p,q}^{\dagger 2} \in [0, 1]$, $\mathbf{U}_I = [U_{i_1}, \dots, U_{i_l}]$ being the $M \times l$ matrix of eigenvectors spanning \mathcal{L}_I , and \circ denoting the Hadamard (element-wise) product.

4. Monitoring of $D_{n,l,p,q}^{\dagger 1, \dots, 3}$ using the Sequential Ranks CUSUM Control Chart

Let us denote the sequential rank of $D_{n,l,p,q}^{\dagger 1, \dots, 3}$ as

$$R_n = 1 + \sum_{r=1}^{n-1} \max \left(0, D_{n,l,p,q}^{\dagger 1, \dots, 3} - D_{r,l,p,q}^{\dagger 1, \dots, 3} \right). \quad (19)$$

The Sequential Ranks CUSUM is then

$$C_n = \max \left(0, C_{n-1} + \frac{R_n}{n+1} - k_{\text{SRC}} \right), \quad n \geq 1 \quad (20)$$

with $C_0 = 0$ and k_{SRC} being a reference constant.

The SRC then signals and a change-point at n is declared if

$$C_n \geq h_{\text{SRC}} \quad (21)$$

holds, i.e., if C_n exceeds a predetermined control limit h_{SRC} .

It can be shown [58] that, given that no change in the monitored signal occurred, the quantities $\frac{R_n}{n+1}$ are independent and discrete uniform on

$$\left\{ \frac{1}{n+1}, \frac{2}{n+1}, \dots, \frac{n}{n+1} \right\},$$

which represents a crucial advantage of the SRC in that it implies that for any k_{SRC} we can obtain the control limit h_{SRC} without the need for any historical training data or further assumptions through simulations as outlined in Algorithm 1.

Algorithm 1: Calculate h_{SRC} for fixed k_{SRC}

- (a) Set a constant N_{SRC}
 - (b) **for** $i = 1$ **to** B **do**
 - i. Construct the set of random variables $\{Y_n\}_{n=1}^{N_{\text{SRC}}}$ as discrete uniform on $\left\{ \frac{1}{n+1}, \frac{2}{n+1}, \dots, \frac{n}{n+1} \right\}$
 - ii. Construct $C_{\text{SRC},n} = \max\{0, C_{\text{SRC},n-1} + Y_n - k_{\text{SRC}}\}$
 - iii. Extract the maximum value of $\{C_{\text{SRC},n}\}_{n=1}^{N_{\text{SRC}}}$
 - end**
 - (c) Set the control limit h_{SRC} as the $B \cdot (1 - ARL_0^{-1})$ ordered extracted maximum value with ARL_0 being the nominal in-control average run length (ARL) (see Appendix A).
-

4. Performance Evaluation

To evaluate and assess the performance and utility of our method we use records which are publicly available through Physiobank [51], a vast and commonly used resource for ECG and other biophysiological data. In particular, since we claim our method to be suitable for both ECG and PPG data, we found the Physionet Challenge 2015 training database (PC15) [50] to be of particular interest as it provides a collection of synchronized ECG and PPG recordings from which we chose a subset similar to the one used in [52]. With PC15 records not being annotated, we purposely chose to limit our evaluation to records containing PVCs (with different frequencies of occurrence) since they can quite accurately be spotted by careful visual inspection.

Furthermore, we evaluate the performance of our simpler method against a competing one proposed by Uus and Liatsis [48], which is related to our work in that it, too, is based on leveraging the change detection capabilities of SSA. For the latter assessment, we use ten cardiologist-annotated ECG records from the St. Petersburg Institute of Cardiological Technics 12-Lead Arrhythmia (INCART) database, which is also publicly available through Physiobank [51]. The additional use of INCART records shall shed light on the robustness of l-SSA-CPD, since as we shall see, contrary to PC15, INCART contains both very noisy signals as well as occasional occurrences of arrhythmias other than PVCs.

Before presenting some results, it seems appropriate to briefly restate the goal of our method, which is to provide a lightweight, model-free tool capable of providing rough assessment and general anomaly detection capabilities under tight resource constraints, e.g., to be used as a pre-screening tool. It is therefore not to substitute for but rather to complement more sophisticated procedures in very much the same way in which it is not a substitute for QRS detectors and should be valued on its own particular merits (which have been discussed in Sections 1 and 2).

4.1. Performance Metrics

In reporting our results we rely on established metrics commonly used in the literature and report *sensitivity* (Se), *specificity* (Sp), and *accuracy* (Acc) defined as

$$Se = \frac{TP}{TP + FN}, \quad (22)$$

$$Sp = \frac{TN}{TN + FP}, \quad (23)$$

$$Acc = \frac{TP + TN}{TP + FP + FN + TN}, \quad (24)$$

with TP, FP, TN, FN being the number of *true positives*, *false positives*, *true negatives*, and *false negatives*, respectively.

Accordingly, *sensitivity* quantifies the ability to correctly detect actual anomalies while vice versa *specificity* quantifies the proportion of non-abnormal segments that are correctly identified as such. *Accuracy*, on the other hand, assesses the overall performance in terms of both correctly identified abnormal and non-abnormal segments.

Note that there is a nonzero detection delay introduced by the use of a control chart. Typically, said delay tends to be longer for nonparametric control charts such as the SRC compared to parametric charts (see, e.g., [58]). Use of the latter however would require imposing a parametric model and therefore inevitably conflict with our goal of minimizing (distributional) assumptions as much as possible.

For an event occurring at time instance n we allow for a certain detection delay τ_d and consider a signal from the control chart as true positive if it falls in the interval $[n, n + \tau_d]$. All results presented here were obtained using $\tau_d = N$, i.e., we allow for a detection delay less or equal to the length of the interval used to construct the initial trajectory matrix \mathbf{X}_B .

Furthermore, note that when directly comparing (synchronized) ECG and PPG signals there is an inherent delay (between the R-peak of the ECG and the respective pulse peak in the PPG) in the PPG signal due to the propagation delay of the pulse pressure wave through the arterial system. This is commonly referred to as *Pulse Arrival Time (PAT)* or *Pulse Transit Time (PTT)* (see, e.g., [9,59]) and illustrated on a short data excerpt (containing a single PVC, highlighted by blue and red backgrounds for ECG and PPG, respectively) in Figure 4. To account for the PTT delay, when dealing with PPG signals we shift the interval $[n, n + \tau_d]$ by $\lfloor 2M/5 \rfloor$, taken to be a rough estimate of the actual PTT.

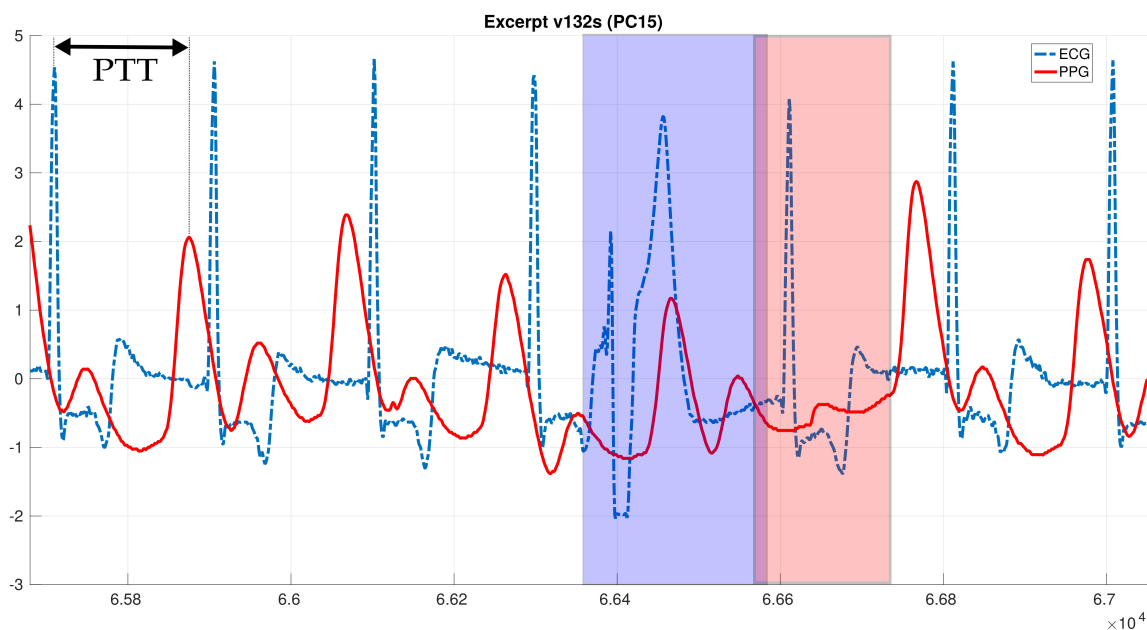


Figure 4. Excerpt of a synchronized recording of ECG (blue dash-dotted) and PPG (red solid) containing a single ectopic beat, highlighted with blue and red backgrounds respectively. Note the shift between the R-peak of the ECG and the respective pulse peak of the PPG, known as Pulse Transit Time (PTT).

4.2. Setup and *l*-SSA-CPD Parameters

The PC15 database [50] provides a collection of ECG and PPG recordings from which we chose a subset similar to the one used in [52]. With PC15 records not being annotated, we purposely chose to limit our evaluation to records containing PVCs (with different frequencies of occurrence), since they can quite accurately be spotted by careful visual inspection. Eventually we included 8 records (composed of two ECG and one PPG signal per record) with varying frequency of PVC occurrence in our analysis. The records are approximately 5 min long with the sampling frequency being 250 Hz, yielding about 75,000 observations each.

Since an in-depth discussion of how to select important SSA tuning parameters, most notably window length M and number of eigentriples used (i.e., selection of l), would be beyond the scope of this paper (see, e.g., [40–42,49,53,54] and references therein), it shall suffice to briefly discuss our settings and the rationale behind them.

Consider a periodic signal with period T , then for SSA to capture the main structure of the signal it is important that M be at least equal to T . Taking into account the physiological limits on HR and the sampling frequency of our signals, $M = 300$ appears to be a safe and reasonable choice. Accordingly, since as discussed in Section 2.1.1 we impose $M \leq N/2$, we set $N = 2M = 600$. Furthermore, we set l to contain the leading l eigentriples such as to account for 92.5% of the data's variance. As for the SRC's control limit, we use $h_{\text{SRC}} = 59.4246$ which we obtained through Algorithm 1 for $B = 10^6$, $N_{\text{SRC}} = 3000$, $ARL_0 = 3000$, $k_{\text{SRC}} = 0.5$.

It shall further be emphasized that, unless otherwise stated, we apply l-SSA-CPD to the raw unfiltered data without any preprocessing steps. This is one further peculiarity that sets this work apart from not only the two competing methods it is benchmarked against in the following subsections but any related work we are aware of. Clearly, suitable preprocessing steps might further enhance performance. The objective here, however, is to ascertain whether or not useful information pertaining to the presence or absence of anomalies) can be obtained by solely applying our l-SSA-CPD with very general parameter settings. A direct performance comparison to MZ is omitted for two main reasons:

- MZ would be computationally prohibitively expensive. Recall that the PC15 records are approximately 75×10^3 samples long, requiring computing the SVD of a 300×301 trajectory matrix, assuming $M = 300$, $N = 600$, $K = N - M + 1$, $Q = 1$ about 74100 times as opposed to just once for l-SSA-CPD (see Figure 2).
- We aim to assess whether, based on its own merits, the performance of l-SSA-CPD suffices to be considered for potential real life applications such as the use case presented in this paper. To further this goal an in-depth comparative analysis to competing algorithms is not required and deemed to be beyond the scope of this paper.

4.3. Performance Evaluation and Comparison on PC15 Data

Table 1 shows the experimental results obtained by applying l-SSA-CP configured as described above to 8 PC15 ECG records with varying length $Q = \{1, 5, 10\}$ of the test matrix $\mathbf{X}_T^{(n)}$.

As elaborated on in Section 3.1, a crucial condition for l-SSA-CPD to work properly by relying solely on the fixed nominal subspace is that the first N samples, which are embedded to form the trajectory matrix \mathbf{X}_B , be an adequate representation of the underlying signal. In other words, we require this initial segment to be free of anomalies. If an anomaly occurs in the first N samples, those samples are to be discarded. This was the case for record t662s, which contains a premature ventricular contraction at about $n = 332 < N$ and required us to discard the first 615 observations. Similar issues were encountered with some of the PC15 PPG traces. More specifically, the first 4000 observations were discarded due to heavy distortions for v253l's as well as as for v368s's PPG signal, as were the first 450 samples of v255l due the presence of an ectopic in the PPG signal. Note that in the case of v255l the ECG traces were not affected, since, consistent with delay due to PTT, the PVC was already over when the recording began.

Examining the entries of Table 1 it is apparent that l-SSA-CPD performs well, especially keeping in mind that in our setup it is applied with fairly general parameters to raw, unfiltered ECG traces. The bottom of the table presents the average performance over the entire 8 records for the three different test statistics $\{D_{n,l,p,q}^{\dagger 1}, D_{n,l,p,q}^{\dagger 2}, D_{n,l,p,q}^{\dagger 3}\}$ and test matrix widths $Q = \{1, 5, 10\}$.

Note how the performance of l-SSA-CPD with test statistic $D_{n,l,p,q}^{\dagger 3}$ is not negatively affected by the at times deteriorated performance of $D_{n,l,p,q}^{\dagger 2}$ and the absence of any benefit from using larger values for Q . These findings corroborate our recommendations made in Section 3.1 to use $D_{n,l,p,q}^{\dagger 3}$ and $Q = 1$, with the latter being in agreement with results reported by other authors (see, e.g., [40,41]). Results obtained using the second ECG trace of the 8 PC15 records were similar and are therefore omitted.

Experimental results obtained by applying l-SSA-CPD to the PPG trace of the same 8 PC15 records are shown in Table 2, again with varying length $Q = \{1, 5, 10\}$ of the test matrix $\mathbf{X}_T^{(n)}$.

Table 1. Detection performance of I-SSA-CPD on PC15 ECG trace I.

Record	Q	1			5			10		
	Statistic	$D_{n,l,p,q}^{\dagger 1}$	$D_{n,l,p,q}^{\dagger 2}$	$D_{n,l,p,q}^{\dagger 3}$	$D_{n,l,p,q}^{\dagger 1}$	$D_{n,l,p,q}^{\dagger 2}$	$D_{n,l,p,q}^{\dagger 3}$	$D_{n,l,p,q}^{\dagger 1}$	$D_{n,l,p,q}^{\dagger 2}$	$D_{n,l,p,q}^{\dagger 3}$
v132s	Se	0.9677	0.9677	0.9677	0.9677	0.8710	0.9677	0.9677	0.6774	0.9677
	Sp	0.9992	0.9991	0.9991	0.9992	0.9988	0.9992	0.9992	0.9997	0.9992
	Acc	0.9992	0.9991	0.9991	0.9992	0.9988	0.9991	0.9992	0.9996	0.9992
v253l	Se	1.0000	1.0000	1.0000	1.0000	0.7922	1.0000	1.0000	0.3247	1.0000
	Sp	0.9987	0.9988	0.9987	0.9987	0.9985	0.9987	0.9987	0.9999	0.9987
	Acc	0.9987	0.9988	0.9987	0.9987	0.9983	0.9987	0.9987	0.9993	0.9987
v255l	Se	0.9844	0.9844	0.9844	0.9844	0.3906	0.9844	0.9844	0.6250	0.9844
	Sp	0.9988	0.9988	0.9988	0.9988	0.9988	0.9988	0.9988	0.9999	0.9988
	Acc	0.9988	0.9988	0.9988	0.9988	0.9984	0.9988	0.9988	0.9996	0.9988
v368s	Se	1.0000	1.0000	1.0000	1.0000	0.7143	1.0000	1.0000	0.7143	1.0000
	Sp	0.9989	0.9985	0.9987	0.9989	0.9994	0.9990	0.9989	0.9995	0.9989
	Acc	0.9989	0.9985	0.9987	0.9989	0.9994	0.9990	0.9989	0.9995	0.9989
v557l	Se	1.0000	1.0000	1.0000	1.0000	0.2500	1.0000	1.0000	0.0000	1.0000
	Sp	0.9993	0.9991	0.9992	0.9993	0.9995	0.9993	0.9993	0.9997	0.9993
	Acc	0.9993	0.9991	0.9992	0.9993	0.9995	0.9993	0.9993	0.9996	0.9993
t662s	Se	1.0000	1.0000	1.0000	1.0000	1.0000	1.0000	1.0000	0.0000	1.0000
	Sp	0.9988	0.9986	0.9987	0.9988	0.9984	0.9987	0.9988	0.9999	0.9988
	Acc	0.9988	0.9986	0.9987	0.9988	0.9984	0.9987	0.9988	0.9998	0.9988
a746s	Se	1.0000	1.0000	1.0000	1.0000	0.8333	1.0000	1.0000	0.6667	1.0000
	Sp	0.9986	0.9987	0.9986	0.9986	0.9990	0.9986	0.9986	0.9997	0.9986
	Acc	0.9986	0.9987	0.9986	0.9986	0.9990	0.9986	0.9986	0.9997	0.9986
v831l	Se	0.9583	0.9583	0.9583	0.9583	0.8750	0.9583	0.9167	0.0417	0.9167
	Sp	0.9992	0.9991	0.9992	0.9992	0.9991	0.9992	0.9992	0.9998	0.9992
	Acc	0.9992	0.9991	0.9991	0.9992	0.9991	0.9992	0.9992	0.9995	0.9992
$\bar{\Sigma}_{\text{ECG}}$	Se	0.9888	0.9888	0.9888	0.9888	0.7158	0.9888	0.9836	0.3812	0.9836
	Sp	0.9989	0.9988	0.9989	0.9989	0.9989	0.9989	0.9989	0.9997	0.9989
	Acc	0.9989	0.9988	0.9989	0.9989	0.9987	0.9989	0.9989	0.9996	0.9989

Comparing the entries of Table 2 with those Table 1 we notice an overall drop in performance. Nevertheless, I-SSA-CPD still manages to provide reasonable results. Furthermore, the recommendation of using $D_{n,l,p,q}^{\dagger 3}$ and $Q = 1$ is shown to hold for the PPG traces as well. Focusing in particular on v368s in Table 2 allows us to highlight an instance of failure and to briefly address its causes. Specifically, after the removal of the first 4000 heavily distorted observations, the record contains 6 PVCs in total, none of which was correctly detected (since the detection delays exceeded the allowed maximum delay and were accordingly counted as false alarms) using $D_{n,l,p,q}^{\dagger 1}$ while the angle-based as well as the augmented statistics $D_{n,l,p,q}^{\dagger 2}$ and $D_{n,l,p,q}^{\dagger 3}$ were both able to detect the first of the 6 PVC events. The detection delay is mainly due the SRC control chart. Accordingly, it would certainly be straightforward to tweak the settings by using an SRC that allows for a more agile response (i.e., lower ARL_0) at the cost of an increase of the false alarm rate (i.e., a decrease in specificity).

A few additional remarks on the three detection statistics $\{D_{n,l,p,q}^{\dagger 1}, D_{n,l,p,q}^{\dagger 2}, D_{n,l,p,q}^{\dagger 3}\}$, however, appear warranted and the fact that in the above example of v368s our augmented statistic $D_{n,l,p,q}^{\dagger 3}$ performs akin to $D_{n,l,p,q}^{\dagger 2}$ rather than $D_{n,l,p,q}^{\dagger 1}$ provides cause for elaborating on the subject. As stated previously, both $D_{n,l,p,q}^{\dagger 1}$ and $D_{n,l,p,q}^{\dagger 2}$ are suitable detection statistics and reliably and readily reflect deviations of new observations from the designated reference subspace. Recalling Equations (15) and (17) note that $D_{n,l,p,q}^{\dagger 2}$ takes values in $[0, 1]$ while $D_{n,l,p,q}^{\dagger 1}$, which our proposed method does, contrary to MZ, not require to be normalized, takes potentially very large values. Accordingly, we propose to use $D_{n,l,p,q}^{\dagger 2}$ as a weighting of $D_{n,l,p,q}^{\dagger 1}$ by combining them taking the Hadamard or element-wise product, which yields $D_{n,l,p,q}^{\dagger 3}$ (see Equation (17)). The benefit of the

proposed augmentation is most readily discernible in Table 2, where we can observe that $D_{n,l,p,q}^{\dagger 3}$ mimics $D_{n,l,p,q}^{\dagger 1}$ in cases where the latter performs well but $D_{n,l,p,q}^{\dagger 2}$ performs very poorly. On the other hand, if the circumstances were reversed (i.e., poorly performing $D_{n,l,p,q}^{\dagger 1}$ and better/well performing $D_{n,l,p,q}^{\dagger 2}$), $D_{n,l,p,q}^{\dagger 3}$ then mimics the better performing angle-based detection statistic. Thus, overall, the proposed augmentation is favorable in that only a minor performance drop (if at all) is experienced when both $D_{n,l,p,q}^{\dagger 1}$ and $D_{n,l,p,q}^{\dagger 2}$ perform well, whereas a lot is gained when they do not.

Furthermore, it should be pointed out that, as has already been observed by other authors (see, e.g., [52]), there are some inconsistencies in the PC15 records in that some of the supposedly synchronized PPG traces exhibit an unusual delay not consistent with the assumption that the PPG pulse peak should have an offset equal to the PTT with respect to the respective R peak in the ECG. Pflugradt et al. attribute this occasional unusual offset to glitches in the original measurement setup (see [52] at 11) and we assume it to have negatively impacted the performance characteristics presented in Table 2 since we allow only for a very limited detection delay τ_d .

Table 2. Detection performance of l-SSA-CPD on PC15 PPG trace.

Record	Q	1			5			10		
	Statistic	$D_{n,l,p,q}^{\dagger 1}$	$D_{n,l,p,q}^{\dagger 2}$	$D_{n,l,p,q}^{\dagger 3}$	$D_{n,l,p,q}^{\dagger 1}$	$D_{n,l,p,q}^{\dagger 2}$	$D_{n,l,p,q}^{\dagger 3}$	$D_{n,l,p,q}^{\dagger 1}$	$D_{n,l,p,q}^{\dagger 2}$	$D_{n,l,p,q}^{\dagger 3}$
v132s	Se	0.7419	0.8387	0.8387	0.7419	0.0000	0.7419	0.7419	0.0000	0.7419
	Sp	0.9994	0.9995	0.9995	0.9994	0.9999	0.9994	0.9994	0.9999	0.9994
	Acc	0.9993	0.9994	0.9994	0.9993	0.9995	0.9993	0.9993	0.9995	0.9993
v253l	Se	1.0000	1.0000	1.0000	1.0000	0.3108	1.0000	1.0000	0.7432	1.0000
	Sp	0.9992	0.9991	0.9991	0.9992	0.9999	0.9992	0.9991	0.9999	0.9991
	Acc	0.9992	0.9991	0.9991	0.9992	0.9993	0.9992	0.9991	0.9997	0.9991
v255l	Se	0.9688	0.9688	0.9688	0.9688	0.4219	0.9688	0.9688	0.4062	0.9688
	Sp	0.9993	0.9993	0.9993	0.9992	0.9999	0.9992	0.9992	0.9999	0.9992
	Acc	0.9992	0.9993	0.9993	0.9992	0.9995	0.9992	0.9992	0.9994	0.9992
v368s	Se	0.0000	0.1667	0.1667	0.1667	0.1667	0.1667	0.0000	0.0000	0.0000
	Sp	0.9978	0.9980	0.9979	0.9978	0.9997	0.9978	0.9977	0.9996	0.9977
	Acc	0.9978	0.9980	0.9979	0.9978	0.9997	0.9978	0.9977	0.9995	0.9977
v557l	Se	1.0000	1.0000	1.0000	1.0000	0.2500	1.0000	1.0000	0.7500	1.0000
	Sp	0.9990	0.9986	0.9988	0.9990	0.9999	0.9990	0.9990	0.9997	0.9990
	Acc	0.9990	0.9986	0.9988	0.9990	0.9998	0.9990	0.9990	0.9997	0.9990
t662s	Se	1.0000	1.0000	1.0000	1.0000	0.0000	1.0000	1.0000	0.0000	1.0000
	Sp	0.9986	0.9986	0.9987	0.9986	0.9999	0.9986	0.9986	0.9998	0.9986
	Acc	0.9986	0.9986	0.9987	0.9986	0.9999	0.9986	0.9986	0.9997	0.9986
a746s	Se	1.0000	1.0000	1.0000	1.0000	0.1667	1.0000	1.0000	0.3333	1.0000
	Sp	0.9980	0.9980	0.9980	0.9980	0.9998	0.9980	0.9980	0.9997	0.9980
	Acc	0.9980	0.9980	0.9980	0.9980	0.9998	0.9980	0.9980	0.9997	0.9980
v831l	Se	0.9583	0.9583	0.9583	0.9583	0.1250	0.9583	0.9583	0.1667	0.9583
	Sp	0.9984	0.9983	0.9983	0.9984	0.9997	0.9984	0.9984	0.9998	0.9984
	Acc	0.9983	0.9983	0.9983	0.9983	0.9995	0.9983	0.9983	0.9995	0.9983
$\bar{\Sigma}_{PPG}$	Se	0.8336	0.8666	0.8666	0.8545	0.1801	0.8545	0.8336	0.2999	0.8336
	Sp	0.9987	0.9987	0.9987	0.9987	0.9998	0.9987	0.9987	0.9998	0.9987
	Acc	0.9987	0.9987	0.9987	0.9987	0.9996	0.9987	0.9987	0.9996	0.9987

Focusing on Table 3, which directly compares our results to those obtained by Pflugradt on the almost identical subset of PC15 records, we observe that on average our l-SSA-CPD outperforms Pflugradt et al.'s Fast Multimodal Ectopic Beat Detector (MEBD) on ECG records, achieving both higher sensitivity and specificity. The case becomes less clear for the respective PPG records, where MEBD exhibits higher sensitivity to the detriment of specificity, which is considerably better using l-SSA-CPD. Again, it shall be emphasized that contrary to MEBD our approach does not require a morphological dissection of the examined signal.

Table 3. Performance comparison of l-SSA-CPD (using $D_{n,l,p,q}^{+3}$, $Q = 1$) and Pflugradt et al.'s [52] Multimodal Ectopic Beat Detector (MEBD) (see [52], Table 6 at 13) on PC15 data.

Method	ECG		PPG	
	Se	Sp	Se	Sp
l-SSA-CPD	0.989	0.999	0.867	0.998
MEBD	0.953	0.989	0.876	0.955

4.4. Performance Evaluation and Comparison on the St. Petersburg INCART Arrhythmia Database ECG Data

As previously mentioned, INCART records provide only ECG traces and furthermore significantly differ from their PC15 counterparts in that they are much longer (30 min as opposed to 5 min), at times very noisy and contain occasional anomalies other than PVCs as well. Therefore, to allow for a fair comparison, we evaluated the performance of l-SSA-CPD with and without an additional preprocessing step consisting of a zero-phase FIR bandpass filter tuned to the interval of $[0.04, 40]$ Hz.

As evidenced by two excerpts from different INCART records shown in Figure 5, the database contains both very contaminated as well as moderately contaminated signals. This directly translates to very good and very poor performance of l-SSA-CPD, as can be seen by looking up the respective records in Table 4. In fact, while our proposed algorithm performs well on the fifth record (and records of similar quality), with sensitivities of 0.82 and 0.99 for the unfiltered and the bandpass-filtered signal, respectively and a specificity of 0.99 for both, its sensitivity drops to rather poor 0.25 and 0.34 for the first record. Note that this was to be anticipated since it is consistent with the limitations of l-SSA-CPD as discussed in Section 3.1. That being said, we would nonetheless like to emphasize the surprisingly good performance of l-SSA-CPD on the ten examined INCART records with the exception of signals $\{I01m, I02m, I04m, I07m\}$ both with and without the additional filtering step. In fact, l-SSA-CPD without BP-filtering still outperforms the manually fine-tuned algorithm of Uus and Liatsis for record I03m and its automatically tuned version additionally for records $\{I08m, I10m\}$. Eventually, with the simple addition of an FIR BP-filtering preprocessing step to l-SSA-CPD, while it still lags behind the algorithm by Uus and Liatsis overall, it manages to outperform its manually fine-tuned version on half of the records, which is remarkable.

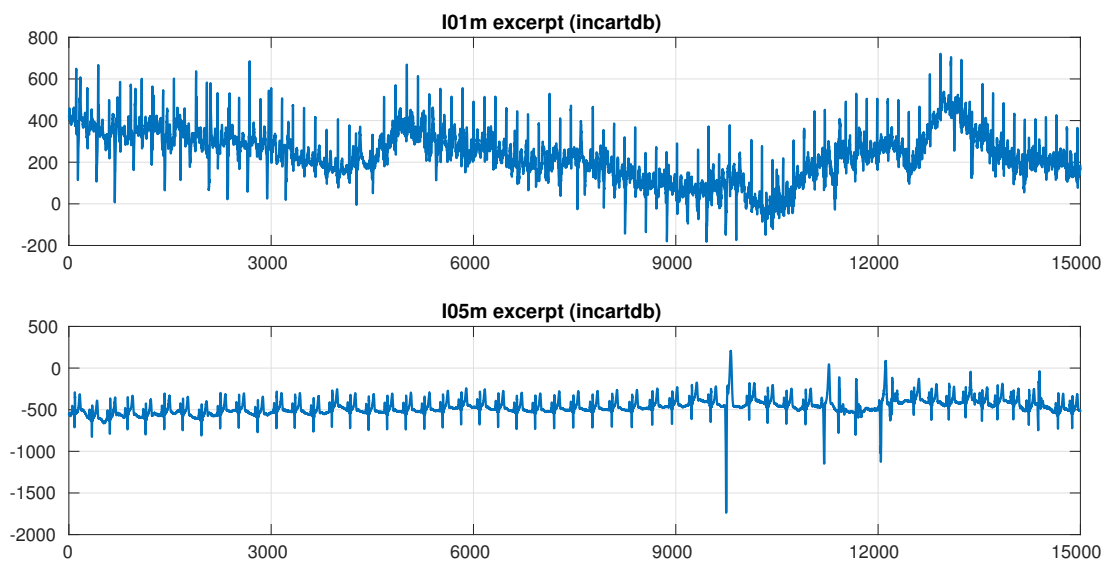


Figure 5. Excerpts of a very noisy I01m (top) and a rather clean I05m (bottom) INCART signal.

Table 4. Performance comparison of l-SSA-CPD (using $D_{n,l,p,q}^{\dagger 3}$, $Q = 1$) and the SSA-based approach by Uus and Liatsis (see [48], Table I) on INCART data.

Record	l-SSA-CPD (unfiltered)		l-SSA-CPD (BP-filtered)		Uus and Liatsis (man. par. adj.)		Uus and Liatsis (aut. par. adj.)	
	Se	Sp	Se	Sp	Se	Sp	Se	Sp
I01m	0.25	0.99	0.34	0.99	0.99	0.95	0.94	0.84
I02m	0.43	0.99	0.24	0.99	0.97	0.93	0.92	0.86
I03m	0.98	0.99	1.00	0.99	0.96	0.95	0.90	0.85
I04m	0.23	0.99	0.58	0.99	0.97	0.92	0.91	0.89
I05m	0.82	0.99	0.99	0.99	0.98	0.94	0.92	0.88
I06m	0.86	0.99	0.97	0.99	0.97	0.96	0.92	0.85
I07m	0.57	0.99	0.74	0.99	0.98	0.93	0.90	0.83
I08m	0.92	0.99	0.99	0.99	0.97	0.91	0.92	0.91
I09m	0.83	0.99	0.89	0.99	0.98	0.91	0.89	0.89
I10m	0.93	0.99	0.98	0.99	0.98	0.93	0.93	0.88

Unfortunately, we are unable to provide detailed commentary on the method proposed by Uus and Liatsis since their paper lacks in clarity and does not provide details pertaining to crucial parts of their algorithm such as how the automatic adjustment of parameters is performed. It is however safe to state that their method is far more complex than ours, for it comprises various stages (such as preprocessing, peak detection, piecewise quadratic polynomial modeling of the R-R series, re-adjustment of parameters, and the creation of a pattern dictionary) that are not required in our method.

5. Discussion and Outlook

In this paper, we have proposed a novel lightweight and model-free approach for the online detection of cardiac anomalies such as ectopic beats in ECG or PPG signals based on the change detection capabilities of Singular Spectrum Analysis (SSA) and nonparametric rank-based cumulative sum (CUSUM) control charts. The procedure is able to quickly detect anomalies without requiring the identification of fiducial points such as R-peaks and is computationally significantly less demanding than previously proposed SSA-based approaches. This is accomplished by modifying the conventional SSA-based change detection algorithm such that the computationally expensive task of computing the SVD is only performed at the very beginning instead of each time a new data point becomes available. Furthermore, our procedure uses more elaborate test statistics that take into account the information derived from the angle between data vectors representing new observations and the subspace representing the signals characteristics as well as the euclidean distances. Lastly, our procedure differs from previous approaches also in that rank-based control limits and the reinitialization of control charts after an anomaly has been detected are used.

Using a set of ECG and PPG records we demonstrated that the direct application of our l-SSA-CPD without any further pre- or post-processing yields not only viable but surprisingly accurate results with an average sensitivity and specificity of 0.9888 and 0.9989 for ECG and 0.8666 and 0.9987 for PPG records, respectively, which compares well and tends to outperform a recently proposed competing approach.

Furthermore, we evaluated the performance of our simpler method against that of a more complex SSA-based approach and were again able to highlight strengths as well as some weaknesses of our proposed method.

With regards to the selection and fine-tuning of SSA-parameters, the performance evaluation on records containing mostly cardiac anomalies other than PVCs and a comparative performance analysis, questions for future works are left open.

Acknowledgments: The author would like to thank the anonymous reviewers for their careful reading of the manuscript and their many insightful comments and suggestions. The work of M. Lang was supported by the ‘Excellence Initiative’ of the German Federal and State Governments and the Graduate School of Excellence Computational Engineering at Technische Universität Darmstadt. The views expressed in this article are solely those of the author in his private capacity and do not necessarily reflect the views of Technische Universität Darmstadt or any other organization.

Conflicts of Interest: The author declares no conflict of interest.

Abbreviations

The following abbreviations are used in this manuscript:

ANN	Artificial Neural Network
ARL	Average Run Length
AV	Atrioventricular Node
CUSUM	Cumulative Sum Control Chart
EKG	Electrocardiography
HR	Heart Rate
INCART	St. Petersburg Institute of Cardiological Technics 12-Lead Arrhythmia Database
l-SSA-CPD	lightweight Singular Spectrum Analysis Change Point Detection
MEBD	Multimodal Ectopic Beat Detector
PAC	Premature Atrial Contraction
PAT	Pulse Arrival Time
PC15	Physionet Challenge 2015 Training Database
PCA	Principal Component Analysis
PPG	Photoplethysmography
PR	Pulse Rate
PTT	Pulse Transit Time
PVC	Premature Ventricular Contraction
SA	Sinoatrial Node
SRC	Sequential Ranks CUSUM Control Chart
SSA	Singular Spectrum Analysis
SVD	Singular Value Decomposition
TERMA	Two Event-Related Moving Averages

Appendix A. CUSUM Control Charts

Consider an observed sequence $\{x_n, n \geq 1\}$ of independent random variables such that $\{x_1, \dots, x_{\tau-1}\} \sim F$ and $\{x_\tau, x_{\tau+1}, \dots\} \sim G$, i.e., a distributional shift $F \rightarrow G$ occurs at time instance τ .

Under the assumption that F and G were normally distributed with known parameters, Page’s CUSUM [60] represents the gold-standard change detection technique and can be computed sequentially as

$$C_0 = 0, \quad C_n = \max\{0, C_{n-1} + x_n - k_C\}, \quad n \geq 1. \quad (\text{A1})$$

The CUSUM signals, thereby declaring a distributional shift to have occurred, if

$$C_n > h_C, \quad (\text{A2})$$

with pre-specified control limit/threshold and reference constant h_C and k_C , respectively. h_C and k_C are chosen such that a nominal average run length (ARL) of ARL_0 is attained when the control chart operates in-control, i.e., without distributional shifts occurring (see, e.g., [61]).

Formally, the in-control ARL is defined as the expected time until a change is signaled under F , i.e.,

$$ARL = E_F \inf\{n > 0 : C_n > h_C\}. \quad (A3)$$

which can be interpreted as akin to setting a nominal type-I error level in hypothesis testing with the closeness of the actual in-control ARL to ARL_0 then being an indicator of the CUSUM chart's robustness [62]. It is well known that, under some regularity conditions, choosing $k_C = \delta/2$, with δ being the shift in the transition $F \rightarrow G$, is optimal [63].

References

1. Anindya, N.; Mukhopadhyay, S.C. Wearable Electronics Sensors: Current Status and Future Opportunities. In *Wearable Electronics Sensors*, 1st ed.; Mukhopadhyay, S.C., Ed.; Springer International Publishing: Cham, Switzerland, 2015; pp. 1–35, ISBN 978-3-31-918190-5.
2. Selke, S. Introduction. In *Lifelogging*, 1st ed.; Selke, S., Ed.; Springer: Wiesbaden, Germany, 2016; pp. 1–21, ISBN 978-3-65-813136-4.
3. Vieau, S.; Iaizzo, P.A. Basic ECG Theory, 12-Lead Recordings, and Their Interpretation. In *Handbook of Cardiac Anatomy, Physiology, and Devices*, 3rd ed.; Iaizzo, P.A., Ed.; Springer International Publishing: Cham, Switzerland, 2015; pp. 321–334, ISBN 978-3-31-919463-9.
4. Gupta, R.; Mitra, M.; Bera, J. *ECG Acquisition and Automated Remote Processing*, 1st ed.; Springer India: New Delhi, India, 2014; ISBN 978-8-13-221556-1.
5. Gacek, A.; Pedrycz, W. *ECG Signal Processing, Classification and Interpretation*, 1st ed.; Springer: London, UK, 2012; ISBN 978-0-85-729867-6.
6. Kiasaleh, K. *Biological Signals Classification and Analysis*, 1st ed.; Springer: Berlin/Heidelberg, Germany, 2015; ISBN 978-3-64-254878-9.
7. Webster, J.G. (Ed.) *Design of Pulse Oximeters*, 1st ed.; CRC Press: Boca Raton, FL, USA, 1997; ISBN 978-0-75-030467-2.
8. Lemay, M.; Bertschi, M.; Sola, J.; Renevey, P.; Parak, J.; Korhonen, I. Application of Optical Heart Rate Monitoring. In *Wearable Sensors*, 1st ed.; Sazonov, E., Neuman, M., Eds.; Academic Press: Cambridge, MA, USA, 2014; pp. 105–129, ISBN 978-0-12-418662-0.
9. Allen, J. Photoplethysmography and its application in clinical physiological measurement. *Physiol. Meas.* **2007**, *28*, R1, doi:10.1088/0967-3334/28/3/R01.
10. Adibi, S. (Ed.) *Mobile Health*, 1st ed.; Springer International Publishing: Cham, Switzerland, 2015; ISBN 978-3-31-912816-0.
11. Holzinger, A.; Röcker, C.; Ziefle, M. (Eds.) *Smart Health*, 1st ed.; Springer International Publishing: Cham, Switzerland, 2015; ISBN 978-3-31-916225-6.
12. Malvey, D.; Slovensky, D.J. *mHealth*, 1st ed.; Springer: New York, NY, USA, 2014; ISBN 978-1-48-997456-3.
13. Lang, M. Heart Rate Monitoring Apps: Information for Engineers and Researchers About the New European Medical Devices Regulation 2017/745. *JMIR Biomed. Eng.* **2017**, *2*, e2, doi:10.2196/biomedeng.8179.
14. Quinn, P. The EU commission's risky choice for a non-risk based strategy on assessment of medical devices. *Comput. Law Secur. Rev.* **2017**, *33*, 361–370, doi:10.1016/j.clsr.2017.03.019.
15. Sperlich, B.; Holmberg, H.C. Wearable, yes, but able...? it is time for evidence-based marketing claims! *Br. J. Sports. Med.* **2017**, *51*, 1240, doi:10.1136/bjsports-2016-097295.
16. Lang, M. Beyond Fitbit: A Critical Appraisal of Optical Heart Rate Monitoring Wearables and Apps, Their Current Limitations and Legal Implications. *Albany Law J. Sci. Technol.* **2017**, *28*, 39–72.
17. Tripathi, O.N.; Ravens, U.; Sanguinetti, M.C. (Eds.) *Heart Rate and Rhythm: Molecular Basis, Pharmacological Modulation and Clinical Implications*, 1st ed.; Springer-Verlag: Berlin/Heidelberg, Germany, 2011; ISBN 978-3-64-217574-9.
18. Jangra, M.; Dhull, S.K.; Singh, K.K. Recent trends in arrhythmia beat detection: A review. In *Communication and Computing Systems*, 1st ed.; Prasad, B.M., Singh, K.K., Ruhil, N., Singh, K., O'Kennedy, R., Eds.; CRC Press: Boca Raton, FL, USA, 2016; pp. 177–183, ISBN 978-1-13-802952-1.

19. Veeravalli, B.; Deepu, C.J.; Ngo, D. Real-Time, Personalized Anomaly Detection in Streaming Data for Wearable Healthcare Devices. In *Handbook of Large-Scale Distributed Computing in Smart Healthcare*, 1st ed.; Khan, S.U., Zomaya, A.Y., Abbas, A., Eds.; Springer International Publishing: Cham, Switzerland, 2017; pp. 403–426, ISBN 978-3-31-958280-1.
20. Elgendi, M.; Eskofier, B.; Dokos, S.; Abbott, D. Revisiting QRS Detection Methodologies for Portable, Wearable, Battery-Operated, and Wireless ECG Systems. *PLoS ONE* **2014**, *9*, e84018, doi:10.1371/journal.pone.0084018.
21. Lemkaddem, A.; Proença, M.; Delgado-Gonzalo, R.; Renevey, P.; Oei, I.; Montano, G.; Martinez-Heras, J.A.; Donati, A.; Bertschi, M.; Lemay, M. An autonomous medical monitoring system: Validation on arrhythmia detection. In Proceedings of the 39th Annual International Conference of the IEEE Engineering in Medicine and Biology Society (EMBC), Jeju Island, Korea, 11–15 July 2017; pp. 4553–4556.
22. Ye, C.; Coimbra, M.T.; Vijaya Kumar, B.V.K. Arrhythmia detection and classification using morphological and dynamic features of ECG signals. In Proceedings of the Annual International Conference of the IEEE Engineering in Medicine and Biology, Buenos Aires, Argentina, 31 August–4 September 2010; pp. 1918–1921.
23. Chang, R.C.H.; Lin, C.H.; Wei, M.F.; Lin, K.H.; Chen, S.R. High-precision real-time premature ventricular contraction (PVC) detection system based on wavelet transform. *J. Sign. Process. Syst.* **2014**, *77*, 289–296, doi:10.1007/s11265-013-0823-6.
24. Yaghouby, F.; Ayatollahi, A.; Bahramali, R.; Yaghouby, M.; Alavi, A.H. Towards automatic detection of atrial fibrillation: a hybrid computational approach. *Comput. Biol. Med.* **2010**, *40*, 919–930, doi:10.1016/j.compbiomed.2010.10.004.
25. Acharya, U.R.; Bhat, B.S.; Iyengar, S.S.; Rao, A.; Dua, S. Classification of heart rate data using artificial neural network and fuzzy equivalence relation. *Pattern Recognit.* **2003**, *36*, 61–68, doi:10.1016/S0031-3203(02)00063-8.
26. Kumar, S.; Bansal, A.; Tiwari, V.N.; Nayak, M.M.; Narayanan, R.V. Remote health monitoring system for detecting cardiac disorders. *IET Syst. Biol.* **2015**, *9*, 309–314, doi:10.1049/iet-syb.2015.0012.
27. Gradl, S.; Kugler, P.; Lohmüller, C.; Eskofier, B. Real-time ECG monitoring and arrhythmia detection using Android-based mobile devices. In Proceedings of the Annual International Conference of the IEEE Engineering in Medicine and Biology Society, San Diego, CA, USA, 28 August–1 September 2012; pp. 2452–2455.
28. Luz, E.J.S.; Schwartz, W.R.; Cámara-Chávez, G.; Menotti, D. ECG-based heartbeat classification for arrhythmia detection: A survey. *Comput. Methods Programs Biomed.* **2016**, *127*, 144–164, doi:10.1016/j.cmpb.2015.12.008.
29. Oresko, J.J.; Jin, Z.; Cheng, J.; Huang, S.; Sun, Y.; Duschl, H.; Cheng, A.C. A Wearable Smartphone-Based Platform for Real-Time Cardiovascular Disease Detection Via Electrocardiogram Processing. *IEEE Trans. Inf. Technol. Biomed.* **2010**, *14*, 734–740, doi:10.1109/TITB.2010.2047865.
30. Amiri, A.M.; Mankodiya, A.K. m-QRS: An efficient QRS detection algorithm for mobile health applications. In Proceedings of the 17th International Conference on E-health Networking, Application & Services (HealthCom), Boston, MA, USA, 14–17 October 2015; pp. 673–676.
31. Kim, Y.J.; Heo, J.; Park, K.S.; Kim, S. Proposition of novel classification approach and features for improved real-time arrhythmia monitoring. *Comput. Biol. Med.* **2016**, *75*, 190–202, doi:10.1016/j.compbiomed.2016.06.009.
32. Tsipouras, M.G.; Fotiadis, D.I. Automatic arrhythmia detection based on time and time-frequency analysis of heart rate variability. *Comput. Methods Programs Biomed.* **2004**, *74*, 95–108, doi:10.1016/S0169-2607(03)00079-8.
33. De Chazal, P.; O'Dwyer, M.; Reilly, R.B. Automatic classification of heartbeats using ECG morphology and heartbeat interval features. *IEEE Trans. Biomed. Eng.* **2004**, *51*, 1196–1206, doi:10.1109/TBME.2004.827359.
34. Pan, J.; Tompkins, W.J. A Real-Time QRS Detection Algorithm. *IEEE Trans. Biomed. Eng.* **1985**, *32*, 230–236, doi:10.1109/TBME.1985.325532.
35. Elgendi, M. Fast QRS Detection with an Optimized Knowledge-Based Method: Evaluation on 11 Standard ECG Databases. *PLoS ONE* **2013**, *8*, e73557, doi:10.1371/journal.pone.0073557.
36. Elgendi, M. TERMA Framework for Biomedical Signal Analysis: An Economic-Inspired Approach. *Biosensors* **2016**, *6*, 55, doi:10.3390/bios6040055.
37. Elgendi, M.; Mohamed, A.; Ward, R. Efficient ECG Compression and QRS Detection for E-Health Applications. *Sci. Rep.* **2017**, *7*, 459, doi:10.1038/s41598-017-00540-x.

38. Elgendi, M.; Al-Ali, A.; Mohamed, A.; Ward, R. Improving Remote Health Monitoring: A Low-Complexity ECG Compression Approach. *Diagnostics* **2018**, *8*, 10, doi:10.3390/diagnostics8010010.
39. Elgendi, M.; Howard, N.; Lovell, N.; Cichocki, A.; Brearley, M.; Abbott, D.; Adatia, I. A Six-Step Framework on Biomedical Signal Analysis for Tackling Noncommunicable Diseases: Current and Future Perspectives. *JMIR Biomed. Eng.* **2016**, *1*, e1, doi:10.2196/biomedeng.6401.
40. Moskvina, V. Application of the Singular Spectrum Analysis for Change-Point Detection in Time Series. Ph.D. Thesis, Cardiff University, Cardiff, UK, 2001.
41. Moskvina, V.; Zhigljavsky, A. An Algorithm Based on Singular Spectrum Analysis for Change-Point Detection. *Commun. Stat. Simul. Comput.* **2003**, *32*, 319–352, doi:10.1081/SAC-120017494.
42. Golyandina, N.; Nekrutkin, V.; Zhigljavsky, A. *Analysis of Time Series Structure: SSA and Related Techniques*, 1st ed.; Chapman and Hall/CRC: Boca Raton, FL, USA, 2001; ISBN 978-1-58-488194-0.
43. Dong, Q.; Yang, Z.; Chen, Y.; Li, X.; Zeng, K. Anomaly Detection in Cognitive Radio Networks Exploiting Singular Spectrum Analysis. In *Computer Network Security. MMM-ACNS 2017. Lecture Notes in Computer Science*; Rak, J., Bay, J., Kottenko, I., Popyack, L., Skormin, V., Szczypiorski, K., Eds.; Springer: Cham, Switzerland, 2017; pp. 321–334, ISBN 978-3-319-19463-9.
44. Yang, Z.; Zhou, N.; Polunchenko, A.; Chen, Y. Singular Spectrum Analysis Based Quick Online Detection of Disturbance Start Time in Power Grid. In Proceedings of the IEEE Global Communications Conference (GLOBECOM) 2015, San Diego, CA, USA, 6–10 December 2015.
45. Zhang, S.; Liu, Y.; Pei, D.; Chen, Y.; Qu, X.; Tao, S.; Zang, S.; Jing, X.; Feng, M. FUNNEL: Assessing Software Changes in Web-Based Services. *IEEE Trans. Serv. Comput.* **2018**, *11*, 34–48, doi:10.1109/TSC.2016.2539945.
46. Georgescu, V.; Delureanu, S.M. Fuzzy-valued and complex-valued time series analysis using multivariate and complex extensions to singular spectrum analysis. In Proceedings of the IEEE International Conference on Fuzzy Systems (FUZZ-IEEE), Istanbul, Turkey, 2–5 August 2015; pp. 1–8.
47. Jarchi, D.; Lo, B.; Wong, C.; Jeong, E.; Nathwani, D.; Yang, G.Z. Gait Analysis From a Single Ear-Worn Sensor: Reliability and Clinical Evaluation for Orthopaedic Patients. *IEEE Trans. Neural. Syst. Rehabil. Eng.* **2016**, *24*, 882–892, doi:10.1109/TNSRE.2015.2477720.
48. Uus, A.; Liatsis, P. Singular Spectrum Analysis for detection of abnormalities in periodic biosignals. In Proceedings of the 18th International Conference on Systems, Signals and Image Processing, Sarajevo, Bosnia and Hercegovina, 16–18 June 2011; pp. 1–4.
49. Sanei, S.; Hassani, H. *Singular Spectrum Analysis of Biomedical Signals*, 1st ed.; CRC Press: Boca Raton, FL, USA, 2015; ISBN 978-1-46-658927-8.
50. Clifford, G.D.; Silva, I.; Moody, B.; Li, Q.; Kella, D.; Shahin, A.; Kooistra, T.; Perry, D.; Mark, R.G. The PhysioNet/Computing in Cardiology Challenge 2015: Reducing False Arrhythmia Alarms in the ICU. *Comput. Cardiol.* **2015**, *42*, 273–276, doi:10.1109/CIC.2015.7408639.
51. Goldberger, A.L.; Amaral, L.A.; Glass, L.; Hausdorff, J.M.; Ivanov, P.C.; Mark, R.G.; Mietus, J.E.; Moody, G.B.; Peng, C.K.; Stanley, H.E. Physiobank, physiotoolkit, and physionet. *Circulation* **2000**, *101*, e215–e220.
52. Pflugradt, M.; Geissdoerfer, K.; Goernig, M.; Orglmeister, R. Fast Multimodal Ectopic Beat Detection Method Applied for Blood Pressure Estimation Based on Pulse Wave Velocity Measurements in Wearable Sensors. *Sensors* **2017**, *17*, 158, doi:10.3390/s17010158.
53. Golyandina, N.; Zhigljavsky, A. *Singular Spectrum Analysis for Time Series*, 1st ed.; Springer: Berlin/Heidelberg, Germany, 2013; ISBN 978-3-64-234912-6.
54. Elsner, J.B.; Tsonis, A.A. *Singular Spectrum Analysis: A New Tool in Time Series Analysis*, 1st ed.; Springer: New York, NY, USA, 1996; ISBN 978-0-30-645472-1.
55. Idé, T.; Inoue, K. Knowledge discovery from heterogeneous dynamic systems using change-point correlations. In *Proceedings of the SIAM International Conference on Data Mining*; Society for Industrial and Applied Mathematics: Philadelphia, PA, USA, 2005; pp. 571–575, ISBN 0898715938.
56. Mohammad, Y.; Nishida, T. Robust Singular Spectrum Transform. In *Next-Generation Applied Intelligence: 22nd International Conference on Industrial, Engineering and Other Applications of Applied Intelligent Systems, IEA/AIE 2009, Tainan, Taiwan*; Chien, B.C., Hong, T.P., Chen, S.M., Ali, M., Eds.; Springer: Berlin/Heidelberg, Germany, 2009; pp. 123–132, ISBN 978-3-64-202568-6.

57. Idé, T.; Tsuda, K. Change-Point Detection using Krylov Subspace Learning. In *Proceedings of the SIAM International Conference on Data Mining*; Society for Industrial and Applied Mathematics: Philadelphia, PA, USA, 2007; pp. 515–520.
58. McDonald, D.R. *A Cusum Procedure Based on Sequential Ranks*. Laboratory for Research in Statistics and Probability; Carleton University: Ottawa, Canada, 1985.
59. Salvi, P. *Pulse Waves*, 1st ed.; Springer: Milan, Italy, 2012; ISBN 978-8-84-702439-7.
60. Page, E.S. Continuous Inspection Schemes. *Biometrika* **1954**, *41*, 100–115.
61. Lucas, J.M. The Design and Use of Cumulative Sum Control Schemes. *Technometrics* **1976**, *14*, 51–59.
62. Chatterjee, S.; Qiu, P. Distribution-free cumulative sum control charts using bootstrap-based control limits. *Ann. Appl. Stat.* **2009**, *3*, 349–369.
63. Reynolds, M.R. Approximations to the average run length in cumulative sum control charts. *Technometrics* **1975**, *17*, 65–71.



© 2018 by the author. Licensee MDPI, Basel, Switzerland. This article is an open access article distributed under the terms and conditions of the Creative Commons Attribution (CC BY) license (<http://creativecommons.org/licenses/by/4.0/>).